References and Notes

1. P. I. Vincent, *Polymer* **13**, 557 (1972); J. A. Odell *et al.*, *J. Polym. Sci.* **24**, 1889 (1986).
2. G. Binnig, C. F. Quate, Ch. Gerber, *Phys. Rev. Lett.* **56**, 930 (1986); S. P. Jarvis, H. Yamada, S.-I. Yamamoto, H. Tokumoto, J. B. Pethica, *Nature* **384**, 247 (1996); M. Radmacher, M. Fritz, H. G. Hansma, P. K. Hansma, *Science* **265**, 1577 (1994).
3. H. Lee *et al.*, *Adv. Mater.* **3**, 316 (1998).
4. U. Dammer *et al.*, *Biophys. J.* **70**, 2437 (1995).
5. P. Hinterdorfer, W. Baumgartner, H. J. Gruber, K. Schilcher, H. Schindler, *Proc. Natl. Acad. Sci. U.S.A.* **93**, 3477 (1996).
6. S. B. Smith, Y. Cui, C. Bustamante, *Science* **271**, 795 (1996).
7. P. Cluzel *et al.*, *ibid.*, p. 792.
8. M. Rief, F. Oesterhelt, B. Heymann, H. E. Gaub, *ibid.* **275**, (1997).
9. M. Rief, M. Gautel, F. Oesterhelt, J. M. Fernandez, H. E. Gaub, *ibid.* **276**, 1109 (1997).
10. A. F. Oberhauser *et al.*, *Nature* **393**, 181 (1998).
11. X. Châtellier, T. J. Senden, J.-F. Joanny, J.-M. Di Meglio, *Europhys. Lett.* **41**, 303 (1998).
12. P. E. Marszalek, A. F. Oberhauser, Y.-P. Pang, J. M. Fernandez, *Nature* **396**, 661 (1998).
13. All of the evaluated molecules show a transition at 275 pN, and the deformation traces scale linearly with the contour length. As has been previously shown (*3, 8, 12*), this is a strict criterion that applies to the stretching of a single polysaccharide.
14. S. Löfas and B. Johnsson, *J. Chem. Soc. Chem. Commun.* **566**, 1526 (1990).
15. Microscope slides (Menzel Gläser, Braunschweig, Germany) and AFM tips (Park Scientific Instruments, Sunnyvale, CA) were incubated with *N′*-[3-(trimethoxysilyl)-propyl]- diethylentriamine (Aldrich) at 90°C for 15 min, rinsed in ethanol, and rinsed in water. The tips and the surfaces were then cured for 30 min at 120°C. The Au surfaces, which were functionalized with amino groups, were prepared by incubating a freshly evaporated Au surface for 30 min with a 100 mM aqueous solution of mercaptoethylamine (Sigma). Carboxymethylated amylose (1 mg/ml) was allowed to react with 1-ethyl-3-(3-dimethylaminopropyl) carbodiimide (EDC) (20 mg/ml) and *N*-hydroxysuccinimide (NHS) (10 mg/ml) (all from Sigma) in phosphate-buffered saline (PBS) at pH 7.4 to introduce succinimide reactive groups along the polysaccharide chain (*14*). This activated polymer was then incubated for 5 min with the amino-silanized glass surface and thoroughly rinsed to remove noncovalently bound molecules. The AFM tip was approached and allowed to react with the amylose so that force versus elongation measurements of the polysaccharide could be recorded. All measurements were recorded in PBS at pH 7.4.
16. To minimize the attachment of multiple amylose strands, which typically occurred at the first approaches of the tip, we let the tip approach the surface step by step, retracting the tip partly after each approach until a binding event was observed upon pulling back. In this so-called "fly fishing mode" (*8*), undesirable multiple bonds can be efficiently avoided.
17. P. G. De Gennes, *J. Phys.* **37**, 1445 (1976).
18. The histogram of the length increase of the amylose strand upon each of these multiple ruptures ranges from 6 to 600 Å. The lower limit of these values is comparable to the length of a stretched sugar ring. Hence, the attachment of a single glucose ring to the surface is capable of holding the entire load applied to the polymer. These steps would result in a plateau if the detachment would be an equilibrium reaction, for example, if the chemical bond could reform before the polymer is pulled away far enough from the surface. Because the detachment of the polymer from the surface is irreversible on the time scale of the experiment and because the AFM has this high spatial resolution, we still see all steps individually (even the small ones, as shown in the enlarged section of the curve in Fig. 2B). The larger steps in the histogram may reflect the unbinding of loops.
19. There are several possible contributions to the width of the distribution. One source is the intrinsic probability distribution for bond rupture. Different angles at which the bonds are loaded may contribute to the broadening of the recorded histogram as well. The rupture force is expected to depend on the loading rate as recently demonstrated for the biotin-streptavidin pair (*22*). This effect was not considered here.
20. Enthalpy of dissociation (in kilojoules per mole) and bond length (in picometers), respectively, are given for the following covalent bonds: Si–C, 318 and 185; Si–O, 452 and 166; C–C, 346 and 154; C–O, 356 and 143; and C–N, 305 and 147 [J. E. Huheey, *Anorganische Chemie* (Walter de Gruyter, Berlin, ed. 3)].
21. E. Evans and K. Ritchie, *Biophys. J.* **72**, 1541 (1997).
22. R. Merkel, P. Nassoy, A. Leung, K. Ritchie, E. Evans, *Nature* **397**, 21 (1999).
23. A. D. Becke, *J. Chem. Phys.* **1993**, 5648 (1993).
24. Gaussian 94, Revision D.4, M. J. Frisch *et al.* [Gaussian, Pittsburgh, PA (1995)].
25. Computations were done with the B3LYP (*23*) density functional method in conjunction with the D95(*d*) basis set as implemented in the Gaussian 94 (*24*) program package on a DEC Alpha 500 workstation.

26. This work was supported by the Deutsche Forschungsgemeinschaft and the Natural Sciences and Engineering Research Council of Canada.

23 December 1998; accepted 5 February 1999

Adaptation of Bulk Constitutive Equations to Insoluble Monolayer Collapse at the Air-Water Interface

J. Patrick Kampf,[1] Curtis W. Frank,[1]* Eva E. Malmström,[2] Craig J. Hawker[2]*

A constitutive equation based on stress-strain models of bulk solids was adapted to relate the surface pressure, compression rate, and temperature of an insoluble monolayer of monodendrons during collapse at the air-water interface. A power law relation between compression rate and surface pressure and an Arrhenius temperature dependence of the steady-state creep rate were observed in data from compression rate and creep experiments in the collapse region. These relations were combined into a single constitutive equation to calculate the temperature dependence of the collapse pressure with a maximum error of 5 percent for temperatures ranging from 10° to 25°C.

Changing the dimensionality of a system can alter its physical properties. For example, many thin polymer films have a glass transition temperature that is much lower than that of the bulk material (*1*), and two-dimensional (2D) melting may occur through a fundamentally different mechanism than the melting of bulk solids (*2*). Despite the inherent differences between 2D and 3D systems, concepts developed for bulk materials can often be extended to describe 2D assemblies. Specifically, the study of monolayer rheology has demonstrated the applicability of continuum concepts to pseudo-2D systems (*3–5*). In addition, investigators have studied the response of Langmuir films to various forms of deformation and have observed elastic (*6*), viscous (*7*), and viscoelastic (*8*) behavior that is analogous to the deformation response of bulk materials. We explored the applicability of phenomenological models developed from the mechanical behavior of bulk solids to the dynamic response of pseudo-2D monolayers at the air-water interface.

[1]Department of Chemical Engineering, Stanford University, Stanford, CA 94305–5025, USA. [2]IBM Almaden Research Center, San Jose, CA 95120–6099, USA.

*To whom correspondence should be addressed.

Surface pressure π versus area A isotherms of Langmuir films are most often thought of as 2D analogs to pressure-volume isotherms of bulk materials, and an equilibrium thermodynamic relation between π and A is assumed. Generally speaking, however, π-A isotherms reflect dynamic, rate-dependent measurements. The parts of the π-A isotherm that will be most affected by the compression rate are those that describe monolayer behavior with long relaxation times. For example, monolayer collapse often occurs in the regime where compression rate becomes an important factor. Several authors have examined the effect of compression rate and temperature T on the collapse of insoluble monolayers. Kato and coworkers (*9*) have shown that compression rate and T alter the collapse pressure of fatty acid monolayers, but they focus mainly on the importance of maintaining a constant strain rate rather than developing a constitutive equation. Duran and coworkers (*10*) have also examined the effect of compression rate and T within the monolayer collapse region of liquid-crystalline polymers, but most of their quantitative work concentrates on relating these parameters to the stress relaxation times. By splitting π into equilibrium and dynamic components,

Downloaded from http://science.sciencemag.org/ on May 2, 2016

Rapp and Gruler (*11*) have developed a quantitative relation between compression rate, T, and π within the monolayer collapse region of a liquid crystal of low molecular weight. Others have used Avrami-type nucleation and growth models (*12*) as well as the Prout-Tompkins equation (*13*) to describe the creep and stress relaxation behavior of insoluble monolayers in the collapse region.

Many types of Langmuir films exhibit collapse behavior that is similar to the stress-strain behavior of polymers when subjected to tensile deformation (*10, 14*). If one identifies π and the change in A as the 2D stress and strain of the monolayer, respectively, then the isotherm features that are analogous to the yield stress, strain softening, and draw stress for many types of bulk polymeric solids become evident. Mechanistic studies of the observed stress-strain behavior of polymer solids have resulted in quantitative relations between stress, strain rate, and T (*15*) that have direct analogies with well-established concepts developed for bulk metals and ceramics (*16*). Our results suggest that monolayer collapse shares similarities with the deformation of bulk metals as well as polymers.

We applied constitutive equations (used to describe the mechanical response of bulk solids) to the collapse of monolayers of poly(benzyl ether) monodendrons with di(ethylene glycol) tails. Monodendrons belong to the group of well-defined highly branched polymers classified as dendrimers (*17*). These monodendrons are surface active, forming monolayers with a collapse behavior (*18–20*) that is qualitatively similar to the Langmuir film deformation response discussed above. Creep and compression rate experiments were analyzed to determine the constants of the constitutive law, which we then used to predict the T dependence of π during collapse. Whereas others have discussed π as a stress (*21*) and change in A as a strain (*9, 22*), we used bulk tensile stress-strain relations to model the collapse behavior of insoluble monolayers at the air-water interface.

In the monolayer, the molecules are arranged so that the globular, hydrophobic monodendron [molecular weight (MW) = 1575] has a diameter-to-height ratio of ~1:2 and is held to the interface by the hydrophilic di(ethylene glycol) tail (MW = 105), which extends into the water. Because the hydrophobic group is much larger than the hydrophilic moiety, the properties of the monodendron, not the tail, determine the monolayer compressibility and molecular area. A sample isotherm at 20°C and at a compression rate of 0.5 cm^2/s is shown in Fig. 1. The initial rise in π at ~120 $Å^2$ indicates the formation of a uniform condensed monolayer. At ~110 $Å^2$, there is an overshoot, or peak, in the isotherm. The peak and plateau at 8 mN/m represent the collapse of the monolayer to a bulk phase.

We propose that the isotherm is analogous to the mechanical response of the class of polymers referred to as tough plastics, which includes a yield stress and a plastic flow region (*15*). The plastic flow region is considered to be a steady-state regime, where the observed stress remains constant when a constant strain rate is applied (or vice versa). For the monolayer system, we suggest that the peak in the isotherm gives the value of the yield stress and that the plateau reflects a region of plastic flow. We do not assert, however, that the molecular mechanisms underlying the observed collapse behavior of the monolayer are equivalent to those thought to occur for tough plastics during tensile deformation. Linear polymers are inherently anisotropic and can form entanglements, whereas dendrimers are globular and show little intermolecular penetration (*23*).

These differences notwithstanding, we propose to extend the scope of materials for comparison to include other types of bulk solids, such as metals. The comparison between metals and a monolayer of organic monodendrons may at first seem to be an odd choice because the fundamental particle in a metal is an atom, whereas the fundamental particle in the monolayer is a dendritic molecule. In addition, the monodendrons are several orders of magnitude larger than metal atoms and have a much higher compressibility. Despite these dissimilar properties, monodendrons are more similar in some ways to metal atoms than to linear polymers. Both monodendrons and metals, for example, are discrete units that cannot entangle. Also, unlike metal atoms and monodendrons, linear polymers sometimes form structures with an intrinsic anisotropy because of their geometry. We are not suggesting that the molecular mechanisms for monolayer collapse are the same as those seen in metals. Instead, we claim that, because of some important similarities in structure, literature on the deformation of metals may aid the understanding of the collapse behavior of dendritic monolayers. Finally, the monolayers are fundamentally different from bulk materials because of their adhesion to the interface, which may result in alternate deformation mechanisms.

We equate π with a 2D stress (*24*), and we define an engineering strain $\alpha = [1 - (A/A_0)]$ with the resulting strain rate $\dot{\alpha}$ of

$$\dot{\alpha} = -\frac{1}{A_0}\frac{dA}{dt} \quad (1)$$

where t is time, A is molecular area, and A_0 is the molecular area at $t = 0$. This strain is not a true strain, and therefore, the strain rate is not a true strain rate (*25*). We compared our monolayer compression results with uniaxial extension rather than compression studies of bulk solids because of the relative abundance of the former in comparison to the latter. Others, however, have applied constitutive equations of the same form as those that are valid for bulk solids under extension to the deformation of solids under uniaxial compression (*26*).

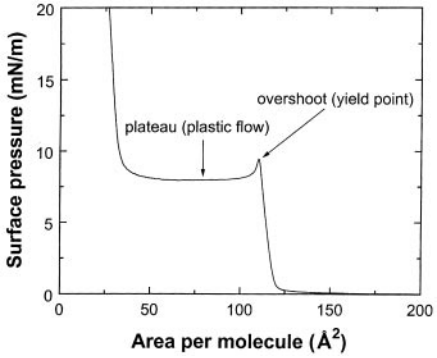

Fig. 1. Typical π-A isotherm for a [G-3]-di(EG) Langmuir film (*19*). The features that are analogous to the stress-strain behavior of a bulk solid are labeled.

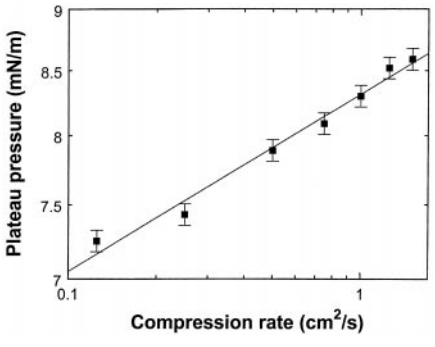

Fig. 2. Power law relation between the plateau pressure of the isotherm and the applied compression rate at 20°C. Squares indicate the experimentally measured values of the plateau surface pressure. The slope of the lines gives $1/n = 0.0717$. Error bars indicate the precision of the surface pressure measurements.

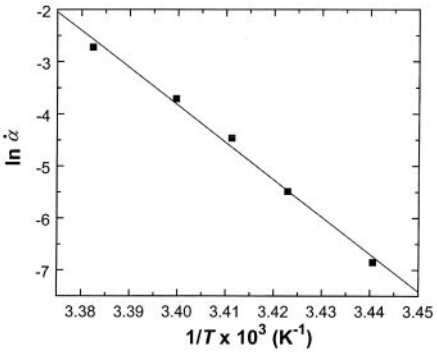

Fig. 3. Arrhenius T behavior of the steady-state creep rate at a constant π of 7 mN/m. Squares indicate the steady-state creep rate as a function of T. The slope of the line gives $E/R = 7.17 \times 10^4$ K. The creep rate is in units of reciprocal minutes.

Downloaded from http://science.sciencemag.org/ on May 2, 2016

Our creep experiments show that the monolayer collapse has a section of steady-state creep where the creep rate is constant, with the strain values for steady-state creep corresponding to the plateau region of the isotherm. The steady-state creep behavior of many metals can be accurately captured with a power law (*16, 27*), and Govaert and coworkers (*28*) have used a power law to model the plastic flow of oriented polyethylene fibers. We conducted experiments to determine the relation between strain rate and the plateau surface pressure π_p. Figure 2 shows π_p as a function of compression rate. The compression rate is proportional to the strain rate, as given by Eq. 1. For the range shown, the relation between π_p and compression rate (strain rate) can be described with a power law as follows:

$$\pi_p = C_1\dot{\alpha}^{1/n} \quad (2)$$

where $n = 13.9$ and C_1 is a T-dependent constant.

Often, the creep rate for plastic flow has an Arrhenius T dependence (*27–29*), and, as shown in Fig. 3, we observed this behavior for the monolayer collapse at a surface pressure of 7 mN/m. Unfortunately, we could only probe a narrow T range because, for $T >$ 22.5°C, the creep rate was faster than the maximum speed of the trough barriers and, for $T <$ 17.5°C, the creep rate was too slow to obtain the desired measurement in a reasonable amount of time. Rearranging Eq. 2 and adding the T dependence, we obtained

$$\dot{\alpha} = C_2\pi_p^n \exp\left(-\frac{E}{RT}\right) \quad (3)$$

where E is the creep activation energy (596 kJ/mol), R is the gas constant, and C_2 is a constant. In Eq. 3, we assume that the strain rate dependence and the T dependence are not coupled. Another implicit assumption is that, in the plastic flow region, the steady-state creep rate of the creep experiments and the applied strain rate of the constant strain rate experiments reflect the same deformation mechanisms.

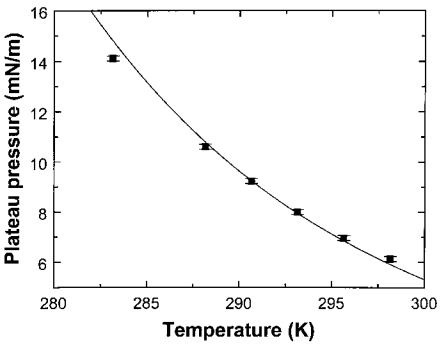

Fig. 4. Comparison between the measured plateau pressure (squares) and the plateau pressure given by Eq. 3 (curve) as a function of T. Error bars indicate the precision of the surface pressure measurements.

We should be able to use Eq. 3 to predict π_p as a function of T. Such a comparison of the calculated values with the measured data should provide a good test of the validity of the assumptions in our model. Figure 4 shows the plateau pressure for T values ranging from 10° to 25°C at a compression rate of 0.5 cm^2/s. With the experimentally determined values of E, n, and C_2, we applied Eq. 3 to predict the T dependence of π_p, as shown in Fig. 4. The maximum error between the experimental data and Eq. 3 is ~5% over the T range shown.

The accuracy of the constitutive law, which applies only to the plastic flow regime, depends on a number of factors. First, the relation between π and strain rate must be accurately described by a power law. Second, the T dependence of the deformation rate must have an Arrhenius form. Third, the stress-strain relation and T dependence must be independent of each other. Finally, the same power law relation and T dependence must hold for both constant compression rate and constant π (creep) experiments. In other words, the deformation mechanisms that underlie the observed steady-state creep behavior must be the same as those that are reflected in the plateau region of the isotherms.

Although Eq. 3 describes the quantitative constitutive relation between stress, strain rate, and T, the nature of the deformation mechanisms underlying the equation remains unclear. Whereas the deformation mechanisms of metals and linear polymers in the plastic flow regime are known, we have insufficient experimental evidence to determine the deformation mechanisms of the monodendron monolayer, which makes insightful comparisons between the activation energies and power law exponents of the different systems difficult. We conclude, however, that the deformation mechanisms in the plastic flow region of the monolayer are related to the formation of a bulk phase at the interface. Monodendron monolayers are unusual Langmuir films, but their observed collapse phenomena are not unique. Our analysis, therefore, may be applicable to other monolayer-forming materials that have a similar amphiphilic balance.

References and Notes

1. O. Prucker *et al.*, *Macromol. Chem. Phys.* **199**, 1435 (1998); J. A. Forrest, K. Dalnoki-Veress, J. R. Dutcher, *Phys. Rev. E* **56**, 5705 (1997); J. L. Keddie, R. A. L. Jones, R. A. Cory, *Faraday Discuss.* **98**, 219 (1994).
2. J. M. Kosterlitz and D. J. Thouless, *J. Phys. C Solid State Phys.* **6**, 1181 (1973); A. P. Young, *Phys. Rev. B* **19**, 1855 (1979); D. R. Nelson and B. I. Halperin, *ibid.*, p. 2457.
3. G. L. Gaines Jr., *Insoluble Monolayers at Liquid-Gas Interfaces* (Interscience, New York, 1966).
4. D. A. Edwards, H. Brenner, D. T. Wasan, *Interfacial Transport Processes and Rheology* (Butterworth-Heinemann, Stoneham, MA, 1991).
5. M. C. Friedenberg, G. G. Fuller, C. W. Frank, C. R. Robertson, *Macromolecules* **29**, 705 (1996); T. Maruyama, G. Fuller, C. Frank, C. Robertson, *Science* **274**, 233 (1996); T. Maruyama, J. Lauger, G. G. Fuller, C. W. Frank, C. R. Robertson, *Langmuir* **14**, 1836 (1998).
6. J. C. Earnshaw and C. P. Nugent, *J. Phys. Condens. Matter* **5**, 1769 (1993); D. Sharpe, J. C. Earnshaw, K. Haig, Y. Li, *Phys. Rev. B* **55**, 6260 (1997).
7. L. E. Copeland, W. D. Harkins, G. E. Boyd, *J. Chem. Phys.* **10**, 357 (1942); M. L. Kurnaz and D. K. Schwartz, *Phys. Rev. E* **56**, 3378 (1997).
8. J. C. Earnshaw and P. J. Winch, *J. Phys. Condens. Matter* **2**, 8499 (1990); A. E. Cárdenas-Valera and A. I. Bailey, *Colloids Surf. A* **79**, 115 (1993); W. Lee, A. R. Esker, H. Yu, *ibid.* **102**, 191 (1995); R. Skarlupka, Y. Seo, H. Yu, *Polymer* **39**, 387 (1998).
9. T. Kato, *Langmuir* **6**, 870 (1990); T. Kato, Y. Hirobe, M. Kato, *ibid.* **7**, 2208 (1991).
10. J. Adams, A. Buske, R. S. Duran, *Macromolecules* **26**, 2871 (1993); H. Fadel, V. Percec, Q. Zheng, R. C. Advincula, R. S. Duran, *ibid.*, p. 1650.
11. B. Rapp and H. Gruler, *Phys. Rev. A* **42**, 2215 (1990).
12. D. Vollhardt and U. Retter, *J. Phys. Chem.* **95**, 3723 (1991); D. Vollhardt, U. Retter, S. Siegel, *Thin Solid Films* **199**, 189 (1991); D. Vollhardt, U. Retter, *Langmuir* **8**, 309 (1992); J. Wagner, T. Michel, W. Nitsch, *ibid.* **12**, 2807 (1996); L. F. Wang, J. F. Kuo, C. Y. Chen, *Mater. Chem. Phys.* **40**, 197 (1995).
13. P. Baglioni, G. Gabrielli, G. G. T. Guarini, *J. Colloid Interface Sci.* **78**, 347 (1980); M. Tomoaia-Cotisel, A. Sen, P. J. Quinn, *ibid.* **94**, 390 (1983); U. Retter and D. Vollhardt, *Langmuir* **8**, 1693 (1992).
14. M. Seitz *et al.*, *Thin Solid Films* **285**, 304 (1996); P. M. Saville, J. W. White, C. J. Hawker, K. L. Wooley, J. M. J. Fréchet, *J. Phys. Chem.* **97**, 293 (1993).
15. L. H. Sperling, *Introduction to Physical Polymer Science* (Wiley, New York, 1992); J. R. Fried, *Polymer Science and Technology* (Prentice-Hall, Englewood Cliffs, NJ, 1995).
16. H. J. Frost and M. F. Ashby, *Deformation-Mechanism Maps: The Plasticity and Creep of Metals and Ceramics* (Pergamon, Oxford, 1982); W. N. Findley, J. S. Lai, K. Onaran, *Creep and Relaxation of Nonlinear Viscoelastic Materials* (Dover, Mineola, NY, 1989); A. J. Krasowsky and L. Toth, *Metall. Mater. Trans. A* **28A**, 1831 (1997).
17. D. A. Tomalia, *Adv. Mater.* **6**, 529 (1994); J. M. J. Fréchet, *Science* **263**, 1710 (1994).
18. J. P. Kampf, C. W. Frank, E. E. Malmström, C. J. Hawker, *Langmuir* **15**, 227 (1999).
19. We used a third-generation poly(benzyl ether) monodendron that was functionalized at the focal point with a single di(ethylene glycol) tail, [G-3]-di(EG) (*18, 20*). A 50 cm by 15 cm symmetric-compression KSV-5000 Langmuir-Blodgett trough (KSV Instruments, Helsinki) was used for all experiments. The subphase was Milli-Q (Millipore, Bedford, MA) deionized water held at a specified constant temperature (±0.2°C) from 10° to 25°C. Solutions of monodendron (~1 mg/ml) in high-performance liquid chromatography–grade chloroform were prepared for spreading. The total amount of amphiphile spread at the air-water interface for each experiment was 94.6 ± 3.6 μg. After a 15- to 20-min wait to allow for solvent evaporation, the barriers were compressed at a constant rate ranging from 0.125 to 1.5 cm^2/s. We measured π with the Wilhelmy plate method (*3*), and the error between experiments was about ±0.1 mN/m. For the creep experiments, the monolayer was compressed at a rate of 1 cm^2/s to π = 7 mN/m, at which point π was held constant and the change in A was recorded.
20. C. J. Hawker and J. M. J. Fréchet, *J. Am. Chem. Soc.* **112**, 7638 (1990).
21. K. C. O'Brien and J. B. Lando, *Langmuir* **1**, 453 (1985); K. Halperin, J. B. Ketterson, P. Dutta, *ibid.* **5**, 161 (1989).
22. T. Kuri, Y. Oishi, T. Kajiyama, *Bull. Chem. Soc. Jpn.* **67**, 942 (1994).
23. C. J. Hawker, E. E. Malmström, C. W. Frank, J. P. Kampf, *J. Am. Chem. Soc.* **119**, 9903 (1997); C. J. Hawker, P. J. Farrington, M. E. Mackay, K. L. Wooley, J. M. J. Fréchet, *ibid.* **117**, 4409 (1995); S. Uppuluri, S. E. Keinath, D. A. Tomalia, P. R. Dvornic, *Macromolecules* **31**, 4498 (1998).
24. Because of our inability to accurately measure the film thickness in situ, we neglected the contribution of thickness changes to the film stress. A precedent

Downloaded from http://science.sciencemag.org/ on May 2, 2016

for our approach is found in tensile stress measurements of bulk materials, which are often made with the assumption of a constant cross-sectional area (*15*). We also ignored the possibility of any spatial gradients in π within the monolayer. Measurements of π were consistently taken from the center of the trough with the compression direction normal to the face of the Wilhelmy plate to ensure reproducibility.
25. Conventionally, the strain rate for the compression or expansion of a monolayer is given by $d(\ln A)/dt$, which is a true strain rate. When dealing with tensile stress-strain experiments conducted on bulk solids, however, the engineering strain $\varepsilon = \Delta L/L_0$ is customarily measured (ΔL, change in length; L_0, original length) (*15*). For such tensile deformation studies, it is necessary to maintain a constant geometry between experiments for the purposes of accurate comparison. Because we draw from the literature developed from the mechanical response of bulk materials to tensile deformation, we use an engineering strain and strain rate. To ensure the validity of comparison between experiments, we spread approximately equal amounts of amphiphilic material at the air-water interface for each experiment.
26. S. Meagher, R. S. Borch, J. Groza, A. K. Mukherjee, H. W. Green II, *Acta Metall. Mater.* **40**, 159 (1992); O. Prakash and D. R. H. Jones, *ibid.*, p. 3443; H. Oikawa, *Mater. Sci. Eng. A* **153**, 427 (1992).
27. W. J. Evans and G. F. Harrison, *J. Mater. Sci.* **18**, 3449 (1983).
28. L. E. Govaert, C. W. M. Bastiaansen, P. J. R. Leblans, *Polymer* **34**, 534 (1993); L. E. Govaert and T. Peijs, *ibid.* **36**, 4425 (1995).
29. C. Y. Cheung and D. Cebon, *J. Rheol.* **41**, 45 (1997).
30. This work was supported by an NIH Biotechnology Training grant and by the Center on Polymer Interfaces and Macromolecular Assemblies, which is sponsored by the NSF Materials Research Science and Engineering Center program under grant DMR-9400354.

4 November 1998; accepted 1 February 1999

Abnormal Spindle Protein, Asp, and the Integrity of Mitotic Centrosomal Microtubule Organizing Centers

Maria do Carmo Avides and David M. Glover*

The product of the *abnormal spindle* (*asp*) gene was found to be an asymmetrically localized component of the centrosome during mitosis, required to focus the poles of the mitotic spindle in vivo. Removing Asp protein function from *Drosophila melanogaster* embryo extracts, either by mutation or immunodepletion, resulted in loss of their ability to restore microtubule-organizing center activity to salt-stripped centrosome preparations. This was corrected by addition of purified Asp protein. Thus, Asp appears to hold together the microtubule-nucleating γ-tubulin ring complexes that organize the mitotic centrosome.

The microtubule-nucleating capacity of the animal cell centrosome requires a ring-shaped complex of proteins associated with γ-tubulin present within the pericentriolar material (PCM) (*1–3*). The PCM contains lattice-like structures in which γ-tubulin has been found associated with pericentrin (*4, 5*). It is not known how the properties of the PCM might change during mitosis specifically to nucleate spindle microtubules.

Asp is a 220-kD microtubule-associated protein (MAP) found at the poles of mitotic spindles in the syncytial embryos of *Drosophila melanogaster* (*6*). It has consensus phosphorylation sites for $p34^{cdc2}$ and mitogen-activated protein kinases and putative binding domains for actin and calmodulin (*6*). Mutations in *asp* result in abnormal spindle morphology leading to mitotic arrest or to a high frequency of meiotic nondisjunction (*7, 8*). Because the mitotic defects of *asp* mutants are best studied in the larval central nervous system, we sought to examine its distribution more carefully in cells of whole-mount preparations of this tissue. We found that Asp became and remained associated with the centrosome throughout mitosis (Fig. 1, A through C). At telophase, it migrated to microtubules on the spindle side of both daughter nuclei (*9, 10*) and was not associated with the centrosome in interphase cells. At all mitotic stages from prophase to anaphase, the Asp protein was asymmetrically localized around the γ-tubulin in the PCM, where it appeared to

Cancer Research Campaign Cell Cycle Genetics Laboratories, Medical Sciences Institute, University of Dundee, Dundee DD1 4HN, UK.

*To whom correspondence should be addressed. E-mail: d.m.glover@dundee.ac.uk

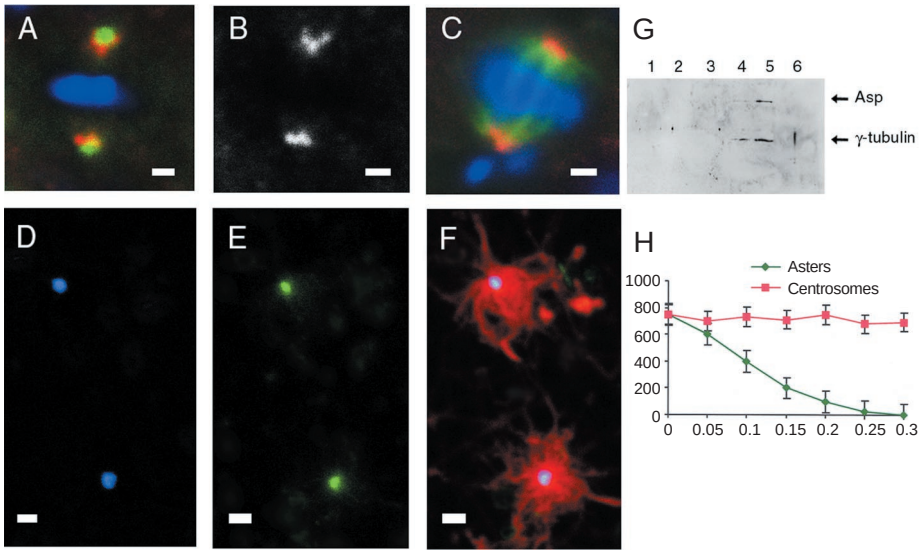

Fig. 1. Antibodies to Asp decorate the centrosome and can block microtubule nucleating activity in vitro. [(A) through (C)] show the immunolocalization of Asp in wild-type neuroblasts from *Drosophila* third-instar larvae. (**A**) Immunolocalization of γ-tubulin (green), Asp (red), and DNA (blue) at metaphase. (**B**) The same cell is shown as in (A) but only with Asp staining. (**C**) An early anaphase cell showing α-tubulin (green), Asp (red), and DNA (blue). (D) through (F) show preparations of centrosomes from *Drosophila* embryos. Shown are (**D**) γ-tubulin (blue), (**E**) Asp (green), and (**F**) a merge of the two previous images also showing the asters of microtubules obtained after incubation with rhodamine-labeled tubulin. (**G**) An immunoblot of the fractions from the final sucrose gradient centrifugation in the centrosome purification procedure (*13*). The 70% sucrose cushion was discarded, and the indicated fractions are the first 6 of a total of 26 in the remaining gradient. Asp and γ-tubulin cosediment in fractions 4 and 5 as indicated. Fraction 5 was used in the experiments here. (**H**) shows antibody competition assays in which centrosomes were first incubated with 0 to 0.3 μg/ml affinity-purified anti-Asp before being used in microtubule nucleation assays and finally being immunostained to reveal γ-tubulin. Preparations were scored for the total number of asters of microtubules and total centrosomes as indicated by foci of γ-tubulin. Scale bars, 10 μm.

Downloaded from http://science.sciencemag.org/ on May 2, 2016

Adaptation of Bulk Constitutive Equations to Insoluble Monolayer Collapse at the Air-Water Interface
J. Patrick Kampf, Curtis W. Frank, Eva E. Malmström and Craig J. Hawker (March 12, 1999)
Science **283** (5408), 1730-1733. [doi: 10.1126/science.283.5408.1730]

Editor's Summary

This copy is for your personal, non-commercial use only.

Article Tools Visit the online version of this article to access the personalization and article tools:
http://science.sciencemag.org/content/283/5408/1730

Permissions Obtain information about reproducing this article:
http://www.sciencemag.org/about/permissions.dtl

Science (print ISSN 0036-8075; online ISSN 1095-9203) is published weekly, except the last week in December, by the American Association for the Advancement of Science, 1200 New York Avenue NW, Washington, DC 20005. Copyright 2016 by the American Association for the Advancement of Science; all rights reserved. The title *Science* is a registered trademark of AAAS.

Downloaded from http://science.sciencemag.org/ on May 2, 2016